

Linear Elastic Fracture Mechanics Pullout Analyses of Headed Anchors in Stressed Concrete

R. Piccinin¹; R. Ballarini, F.ASCE²; and S. Cattaneo³

Abstract: The results of research initiated in the early 1980s led to the replacement of plasticity-based design guidelines for the load-carrying capacity of headed anchors embedded in concrete with those developed using fracture mechanics. While provisions are available in the design codes that account for the presence of tensile fields causing concrete cracking, no provisions are available for anchors embedded in prestressed concrete. This paper presents the results of linear elastic fracture mechanics (LEFM) analyses and of a preliminary experimental investigation of the progressive failure of headed anchors embedded in a concrete matrix under compressive or tensile prestress. The model predicts an increase (decrease) in load-carrying capacity and ductility with increasing compressive (tensile) prestress. It is shown that despite neglecting the dependence on size of concrete fracture toughness, LEFM predicts with remarkable accuracy the functional dependence of the ultimate capacity on prestress.

DOI: 10.1061/(ASCE)EM.1943-7889.0000120

CE Database subject headings: Anchors; Axisymmetry; Finite element method; Prestressed concrete; Cracking; Tensile strength.

Author keywords: Headed anchors.

Introduction

Steel headed anchors embedded in a concrete matrix are widely used in structural engineering applications. Their load-carrying capacity can be predicted with confidence for cases in which the stem yields; it is simply equal to the yield stress of the steel multiplied by the cross-sectional area of the stem. Predicting the maximum load achieved during the progressive failure of the concrete, however, is much more difficult. Numerous analytical, computational, and experimental studies (Klinger and Mendonca 1982; Krenchel and Shah 1985; Farrow and Klinger 1995; Ballarini et al. 1985; Eligehausen and Sawade 1989; Ozbolt and Eligehausen 1992; Karihaloo 1996; Farrow et al. 1996; Elfgren 1998; Ozbolt et al. 1999; Eligehausen et al. 2006; Cattaneo 2007) have been performed to guide the development of reliable design formulas, for cases involving concrete failure, of isolated and interacting anchors subjected to various loading configurations. Before the early 1980s, predictions relied on plasticity-type models, for which the capacity (limit load) of the anchor is equal to the force produced by a prescribed traction distribution acting along the surface of a conical section of concrete with an assumed shape.

ACI Committee 349 (1989), for example, previously allowed

¹Research Assistant, Dept. of Civil Engineering, Univ. of Minnesota, MN 55455-0116 (corresponding author). E-mail: picci007@umn.edu

²James L. Record Professor and Head, Dept. of Civil Engineering, Univ. of Minnesota, MN 55455-0116. E-mail: broberto@umn.edu

³Assistant Professor, Dept. of Structural Engineering, Politecnico di Milano, Piazza L. Da Vinci, Milan 20133, Italy. E-mail: cattaneo@stru.polimi.it

Note. This manuscript was submitted on January 12, 2009; approved on November 16, 2009; published online on November 19, 2009. Discussion period open until November 1, 2010; separate discussions must be submitted for individual papers. This paper is part of the *Journal of Engineering Mechanics*, Vol. 136, No. 6, June 1, 2010. ©ASCE, ISSN 0733-9399/2010/6-761-768/\$25.00.

the capacity of a headed anchor of diameter c , embedded at a depth d , to be determined using a uniform tensile stress, f_t , acting on the projected area of a conical failure surface inclined at 45° with respect to the free surface. The limit load derived using this model and the empirical relation between the tensile and compressive strengths, $f_t = 4\sqrt{f'_c}$, is given by

$$P_{u,ACI} = \phi f_t \pi d^2 \left(1 + \frac{c}{d}\right) = (\phi 4\sqrt{f'_c}) \pi d^2 \left(1 + \frac{c}{d}\right) \approx f_t d^2 \quad (1)$$

where ϕ = strength reduction factor. Experimental data (Klinger and Mendonca 1982; Ballarini et al. 1985; Eligehausen and Sawade 1989; Ozbolt and Eligehausen 1992; Ozbolt et al. 1999) has convincingly demonstrated that the d^2 -dependence demanded by dimensional consistency and expressed by Eq. (1) is incorrect and unconservative for typical embedment depths. Realizing that the failure of headed anchors reflects a progressive crack propagation process, Ballarini et al. (1985), Eligehausen and Sawade (1989), and Ozbolt and Eligehausen (1992) approached the problem of predicting the ultimate load capacity of headed anchors, and in particular the dependence of pullout force on embedment depth, using fracture mechanics. Linear elastic fracture mechanics (LEFM) is a one-parameter system for which the equilibrium nominal stress, σ_N , corresponding to a crack of length l , is proportional to $K_c l^{-1/2}$, where K_c is the fracture toughness (which can be expressed in terms of the critical energy release rate, G_c , and Young's modulus, E , through the Irwin relation, $G_c = K_c^2/E$). Dimensional consistency demands that the pullout force be of the form

$$P_{u,LEFM} \approx K_c d^{3/2} \approx k_c \cdot \sqrt{f'_c} \cdot d^{3/2} \quad (2)$$

The experimentally determined proportionality factor k_c that relates the fracture toughness to the compressive strength was introduced by Fuchs et al. (1995) in the concrete capacity design (CCD) method and set equal to a constant value, independent of the embedment depth of the anchor.

The $d^{3/2}$ -dependence and the CCD method take into account the concrete's size dependent fracture toughness and have been validated through numerous experiments. As a result design formulas based on fracture mechanics have been incorporated into design codes and provisions [i.e., Comité Euro-International du Béton (CEB) 1997; ACI Committee 349 2006; ACI Committee 318 2008].

After an extensive experimental program (Eligehausen and Balogh 1995), the capacities obtained from Eq. (2) were reduced to account for cases where cracking due to external loads (i.e., tension zones, negative moment loading conditions) or imposed deformations (i.e., creep, shrinkage, temperature) are expected in the region where the anchor is placed. For example, relative to the uncracked condition a 25% reduction in ultimate load-carrying capacity for cracked concrete in ACI Committee 318 (2008) is quantified. In most of the tests performed to assess the effect of concrete cracking (Eligehausen et al. 2004), cracks were performed in a reinforced concrete matrix and their width was kept nearly constant by constraining the specimen. Subsequently, the anchors were monotonically loaded to failure. Concrete cone failures were observed; compared to the uncracked case, the load-displacement curves showed to be flatter, the ultimate load was markedly reduced, and the displacement at failure increased. Even though representative of many practical applications, it appears that the presence of reinforcement and the restraint applied to the concrete matrix might not provide a complete understanding of the effect of transversal tension on the ultimate load-carrying capacity of the inserts.

The problem of predicting the load-capacity of cast-in-place inserts placed in precast, prestressed concrete members to facilitate connections between different elements has received much less attention. In fact, ACI 318 does not provide modifications to Eq. (2) that account for prestress. The connection of cast-in-place concrete diaphragms or floor beams to precast concrete girders in bridges is but one example of applications involving prestress. Baran et al. (2006) performed experiments on different types of cast-in-place inserts to determine the influence of reinforcement and prestress. As expected, they observed that the presence of a prestressing force in the direction orthogonal to the axes of the inserts embedded in reinforced concrete resulted in an increase in load capacity and ductility.

Research Significance

Because of the lack of a design formula for the prediction of the load-carrying capacity of headed anchors embedded in a prestressed concrete matrix and the actual experimental nature of the code provisions for the capacity of inserts in cracked concrete, this paper presents the results of LEFM analyses of the progressive pullout of headed anchors embedded in a stressed matrix. The effects of stresses on the load-carrying capacity and ductility are calculated in terms of the to-be-defined brittleness number. Also presented are the results of a preliminary experimental program aimed at assessing the LEFM model's prediction of the effects of prestress on ultimate capacity.

LEFM Model and Nondimensional Parameters

Plasticity-based and LEFM models provide useful upper bounds on the strength of a structure containing a crack. The smooth transition from ductile to brittle failure can be characterized using

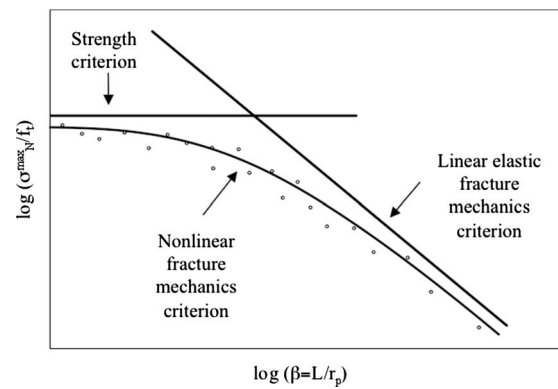


Fig. 1. Nominal strength versus structural size

nonlinear fracture mechanics models, including those of the cohesive zone type. These involve the parameter β introduced by Cherepanov (1979) defined by

$$\beta \equiv \frac{L}{r_p} \approx \frac{f_r^2 L}{K_c^2} \quad (3)$$

where r_p = length of the “process zone” (microcracking and aggregate interlock) that develops in the vicinity of a very long crack and L is a characteristic dimension of the structure. We note that β is referred to by the concrete fracture mechanics community as the brittleness number [Bazant and Planas (1998); note that Carpinteri (1982) defined the brittleness number as $s = \beta^{-1}$]. It is important to note that the brittleness number is simply the size of the plastic zone relative to one or more characteristic dimensions of the structure, and that the interaction between a relatively large plastic zone and free boundaries can be complex. Therefore the value of brittleness assigned to a specimen configuration through the use of a particular structural dimension in Eq. (3) may not be representative of the brittleness of a different configuration comprised of the same material. For example, as pointed out by Bazant valid toughness testing requirements for notched beam-like specimens, where the characteristic dimension L is taken as the beam depth, suggest the approximate constraint $\beta \geq 2.5$. However, for concrete anchors applications, where the characteristic length L can be taken as the embedment depth (which is typically much smaller than the dimensions of a beam structure) it is not uncommon to find values of $\beta \leq 1$ (Elfgren and Ohlsson 1992).

Fig. 1 illustrates that the brittleness number determines whether failure is of the strength limited ductile type (defined in terms of some normalized maximum nominal stress, σ_N^{\max}), or of the toughness limited brittle type. Noting that L is proportional to d , and that any choice of nominal area scales as d^2 , plasticity predicts a size-independent strength, while LEFM predicts a $1/\sqrt{\beta}$ dependence of strength. The design formulas that are now available in design codes for headed anchors embedded in non-stressed concrete are the fruits of LEFM and nonlinear fracture mechanics models that have captured the transition illustrated in Fig. 1. As stated previously, while experiment-based formulas have been developed for cracked concrete conditions, no formulas are currently available that account for prestress within the concrete; hence the motivation behind the LEFM model presented next.

Fig. 2(a) shows the cross section of the axisymmetric configuration considered in this study. The headed anchor, embedded at a depth d within a matrix stressed to a level, σ , is represented [as was done in Ballarini et al. (1985, 1987), and Vogel and Ballarini

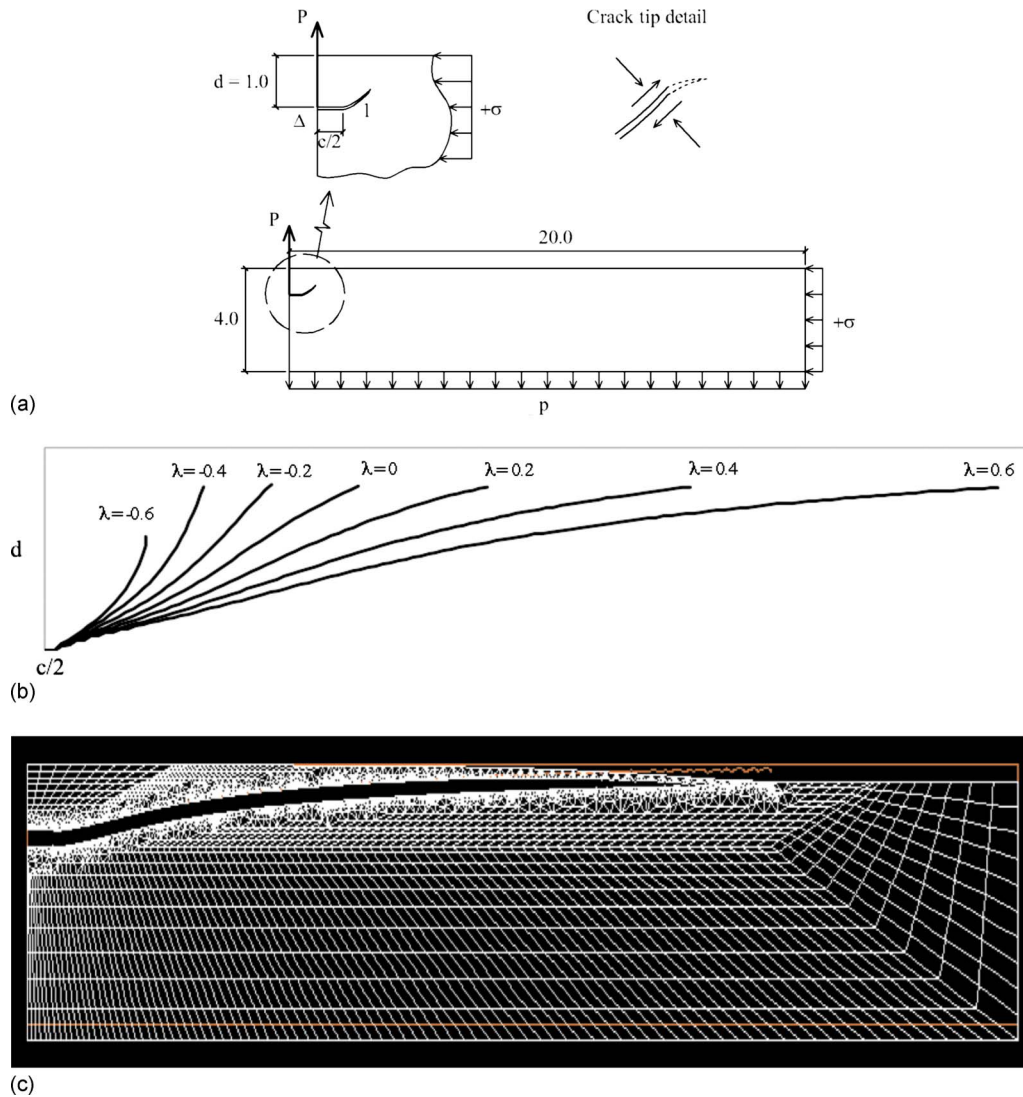


Fig. 2. (a) Cross section of the axisymmetric headed anchor model under prestress; the axis of rotation/symmetry is represented by the left edge of the section; (b) crack paths as function of the applied stress ($\beta=6.25$ and $d/c=10$); and (c) finite-element discretization of the axisymmetric headed anchor ($d/c=1$) with detail of the deformed configuration at the end of the crack propagation simulation

(1999)] by a discontinuity of diameter c with a rigid top surface and a traction-free lower surface. The stem is not considered. The pullout load (P) is represented by the resultant reactive force on the top surface of the discontinuity produced by a uniform stress (p) applied along the bottom surface of the cylindrical model. The curvilinear distance of the traction-free crack front from the edge of the anchor is defined by l , and the normalized level of stress is defined as $\lambda = \sigma/f_t$ (note that for the compressive case $\lambda > 0$, while for the tension case $\lambda < 0$).

As it is typically assumed in LEFM analyses of brittle and quasi-brittle materials, the crack is propagated when the Mode I stress intensity factor K_I for a given crack length l reaches a value equal to the fracture toughness K_{IC} of the material. FRANC-2D (1997), a program that possesses automatic remeshing capabilities, was used to calculate the stress intensity factors and crack extension direction of the propagating front. A representative deformed finite-element mesh of this configuration is shown in Fig. 2(c). The stress intensity factors were determined using the displacement correlation method (Barsoum 1976), and the crack path was selected using the maximum hoop stress criterion (Broek 1986).

We note that the model's predictions for ultimate capacity and ductility should be considered from the perspective of (1) an idealized geometry that neglects the effects produced by the precise geometry of embedded anchors and the radial cracking that often accompanies the crack propagation simulated in this work and (2) a homogeneous material that neglects the intrinsic heterogeneity of concrete.

The compressive stress produces two effects that increase the load-carrying capacity and the ductility of the anchor. As shown in a close-up view of the tip of the traction-free crack [Fig. 2(a)], the first contribution is made by the component of the prestress acting perpendicular to the line defining the crack surfaces (the components of stress associated with the applied loading are not shown in this figure). This stress resists crack opening, and in turn crack extension. The second contribution, also shown in the figure, is from the component of the prestress in the direction parallel to the line defining the crack surfaces, which increases the algebraic value of the Mode II stress intensity factor, changes the direction of maximum hoop stress, and as shown in Fig. 2(b), steers the crack front parallel to the free surface and the direction of the prestress. Tensile prestress produces the opposite effects,

facilitating crack opening, and steering the crack front toward the free surface.

Following Vogel and Ballarini (1999), linearity and dimensional consistency demand that under a given stress level, σ , the load associated with an equilibrium crack length, l , is of the form

$$P_{LEFM} = f_1 \left(\frac{l}{d}, \frac{d}{c}, \nu \right) \cdot K_{Ic} \cdot d^{1.5} + f_2 \left(\frac{l}{d}, \frac{d}{c}, \nu \right) \cdot \sigma \cdot d^2 \quad (4)$$

where ν = Poisson's ratio (assumed equal to 0.2). The normalized maximum load can be written in terms of β and λ as

$$\begin{aligned} \frac{P_{u,LEFM}}{f_t \cdot d^2} &= \max \left[f_1 \left(\frac{l}{d}, \frac{d}{c}, \nu \right) \cdot \frac{K_{Ic}}{f_t \cdot d^{0.5}} + f_2 \left(\frac{l}{d}, \frac{d}{c}, \nu \right) \cdot \frac{\sigma}{f_t} \right] \\ &= \max \left[f_1 \left(\frac{l}{d}, \frac{d}{c}, \nu \right) \cdot \frac{1}{\sqrt{\beta}} + f_2 \left(\frac{l}{d}, \frac{d}{c}, \nu \right) \cdot \lambda \right] \end{aligned} \quad (5)$$

The plasticity-based normalized capacity predicted by the obsolete ACI Committee 349 (1989) guidelines can be written as

$$\frac{P_{u,ACI}}{f_t \cdot d^2} = \phi \pi \cdot \left(1 + \frac{c}{d} \right) \quad (6)$$

Experimental Program

In this section the procedures and the experimental setup used to assess the predictions of the LEFM simulations are described. The aim of the experimental program was to determine the ultimate load-carrying capacity (pullout load) and the load versus displacement behavior of headed anchors embedded in both unstressed and prestressed concrete matrix.

The experimental program employed a normal-strength concrete [cylindrical strength of 4.73 ksi (32.59 MPa) and cubic strength of 5.26 ksi (36.30 MPa)]. The compressive strength was evaluated on both cylindrical [diameter of 3.94 in. (100 mm) and height of 7.87 in. (200 mm)] and cubic specimens [5.9 in. (150 mm) sideways]. Standard size cylinders [ASTM C31 (ASTM 2002) and C496/C496M (ASTM 1996)] were tested to obtain the Young's modulus and the uniaxial tensile strength of the material (Brazilian splitting test). After averaging, the values obtained were 3,408 ksi (23,500 MPa) and 417 psi (2.88 MPa), respectively. The mix components of the concrete used for this investigation were a Portland cement CEM I 52.5 R, according to ENV 197/1 European Standard, and a natural river aggregate (maximum size of 25 mm). No superplasticizers were used. The concrete had an aggregate/cement ratio of 6.24 and a water/cement ratio of 0.7.

All specimens were prepared using steel molds and consolidated with a high frequency vibrating table, removed from the mold after 24 h, and air cured at a temperature of about 22°C. The tests were performed at an age of concrete between 28 and 35 days. The concrete specimens consisted of concrete blocks of two sizes, 39.37 × 39.37 × 7.87 in. (1 × 1 × 0.2 m) and 49.21 × 61.02 × 9.45 in. (1.25 × 1.55 × 0.24 m).

Four anchors were placed in each specimen at a sufficient distance among them to avoid interactions and from the edges of the specimens to avoid edge effects or undesired modes of failure (i.e., concrete blow-out). The concrete anchors had a stem diameter of 0.5 in. (12.7 mm) and a head diameter of 0.98 in. (25 mm). They had an ultimate strength of 65 ksi (450 MPa) and a yield characteristic strength of 51 ksi (350 MPa). Table 1 lists the properties of the materials employed in the experimental program.

Table 1. Material Properties [Units in ksi (MPa)]

Material	Property	Value
Concrete	28 days cylinder strength, $f_c^{28d_{cyl}}$	4.73 (32.59)
	28 days cubic strength, $f_c^{28d_{cube}}$	5.26 (36.30)
	21 days cylinder strength, $f_c^{21d_{cyl}}$	3.90 (26.90)
	21 days cubic strength, $f_c^{21d_{cube}}$	4.70 (32.40)
	Tensile strength, f_t	0.42 (2.88)
	Elastic modulus, E	3,408 (23,500)
Steel	Yield strength, 0.2% offset, f_y	51 (350)
	Ultimate strength, f_u	65 (450)

All the anchors were cast-in-place during a single cast. Wood formworks were used as a support for the anchors during the casting procedure so that they could easily be positioned at different embedment depths. In the tests, two different embedment depths were employed: 0.98 and 1.97 in. (25 and 50 mm). These values were preliminarily chosen to obtain embedment depth versus head diameter ratios (namely, d/c) equal to 1 and 2, respectively.

A representation of the testing machine employed in the experiments is shown in Fig. 3. The load was applied by means of a hydraulic jack with a reaction frame. The reaction frame consisted of a steel beam, with the section shown in Fig. 3. The load was applied through a steel rod connected to the reaction frame at the top and to a special device that connected the anchor at the end. The tests were load controlled and the relative displacements between the anchors and the upper surface of the concrete blocks were monitored by two LVDTs [± 0.2 in. (± 5 mm)] symmetrically positioned at a distance of 10.4 in. (264.2 mm) for short embedment depths and 15.2 in. (385 mm) for larger embedment depths from the axis of the anchor.

The effect of prestress was simulated by applying biaxial compression along the sides of the specimens. As shown in Figs. 4 and 5, the compression was applied by means of horizontally oriented hydraulic jacks inserted in a specially built-in reaction frame. The steel beams used to build the reaction frame were tied

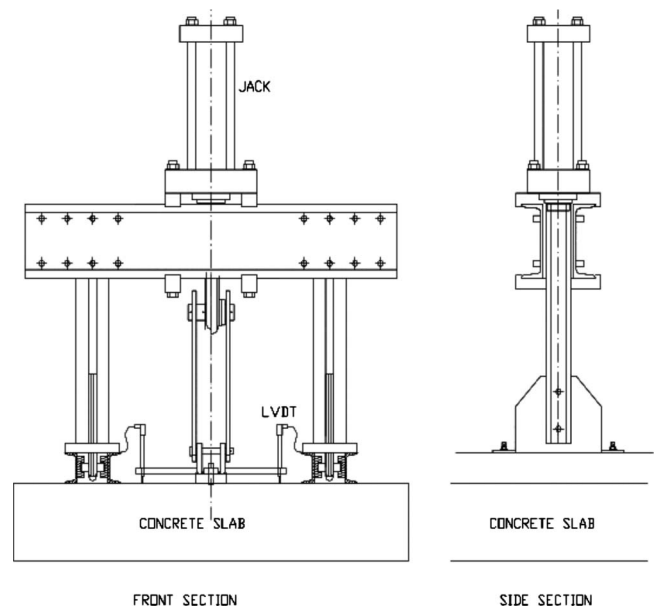


Fig. 3. Testing machine used for the extraction of the concrete headed anchors and location of the LVDTs



Fig. 4. Detail of the built-in frame for the application of biaxial compression

together in the two plane directions by using six special Dividag tying bars. On the two sides of the specimens where the hydraulic jacks were acting, two additional steel beams were used to uniformly distribute the horizontal pressure. The other sides of the specimens were loaded by contrast through the reaction frame. To allow for a more uniform load distribution, a 0.4 in. (10 mm) layer of rubber band was positioned between the specimens and the frame.

The pullout tests were performed for each embedment depth in unconfined concrete, while biaxial compression was applied only to anchors with $d/c=2$ (Table 2). The tests in confined concrete were performed considering three different amount of compression: 5, 7.5, and 10% of the cylindrical compressive strength of the concrete measured at 21 days [3.9 ksi (26.9 MPa)]. That is, 0.19 ksi (1.34 MPa), 0.29 ksi (2.02 MPa), and 0.39 ksi (2.69 MPa), respectively. The applied compression was constantly monitored before and after each pullout test with standard manometers.

Results

Ultimate Load-Carrying Capacity: Finite-Element Model

Representative results for f_1 [Eq. (4)] as functions of crack length are shown in Fig. 6. The maxima of each curve were used to establish Fig. 7, where the capacities predicted by Eqs. (2) and (5) were normalized by the ultimate capacity at the embedment depth $d/c=10$. With an experimentally calibrated constant factor, k_c , embedded in its formula, and with the assumption that exact pull-out forces are being provided, the ACI 318 code-based prediction



Fig. 5. Detail of the built-in frame with the testing machine

Table 2. Experimental Program Details and Parameters

Test	Embedment depth, d , [in. (mm)]	Head diameter, c , [in. (mm)]	d/c	Applied prestress, σ_c , [ksi (MPa)]
1	2.12 (53.85)	0.98 (25)	2.15	0 (0)
2	1.97 (50.04)	0.98 (25)	2.00	0 (0)
3	2.06 (52.32)	0.98 (25)	2.09	0 (0)
4	1.88 (47.75)	0.98 (25)	1.91	0 (0)
5	0.93 (23.62)	0.98 (25)	0.95	0 (0)
6	0.97 (24.64)	0.98 (25)	0.99	0 (0)
7	0.96 (24.38)	0.98 (25)	0.97	0 (0)
8	0.91 (23.11)	0.98 (25)	0.92	0 (0)
9	1.95 (49.53)	0.98 (25)	1.98	0.20 (1.34)
10	2.00 (50.80)	0.98 (25)	2.04	0.20 (1.34)
11	2.19 (55.63)	0.98 (25)	2.22	0.39 (2.69)
12	1.92 (48.77)	0.98 (25)	1.95	0.39 (2.69)
13	1.97 (50.04)	0.98 (25)	2.01	0.29 (2.02)
14	1.91 (48.51)	0.98 (25)	1.94	0.29 (2.02)
15	1.93 (49.02)	0.98 (25)	1.96	0.20 (1.34)
16	2.06 (52.32)	0.98 (25)	2.09	0.29 (2.02)

is ideally represented by a horizontal line while results from the LEFM incremental analyses show that the ultimate load-carrying capacity slightly decreases with increasing d/c .

Fig. 7 provides valuable information. First, and as clearly demonstrated by previous experimental investigations (Ozbolt and Eligehausen 1992), it shows that for relatively large embedment depths there is very little difference between the LEFM predictions and the ACI 318 code-based formula. For relatively small embedment depths, however, the code-based formula is associated with pullout forces that are lower than the upper bound LEFM predictions. Fig. 7 thus shows that predicting the ultimate capacity for $d/c < 2$ requires nonlinear fracture mechanics models that account for the process zone that accompanies a propagating crack front.

The effects of prestress on load-carrying capacity for selected values of λ and β are shown in Fig. 8(a) ($d/c=1$) and Fig. 8(b) ($d/c=2$). As indicated by LEFM-derived Eq. (5), the load-carrying capacity varies linearly with prestress. Fig. 9 illustrates Eq. (5) prediction of an inverse square root decrease in strength with increasing brittleness. For $0.1 \leq \beta \leq 10$ and $0 \leq \lambda \leq 1$, the following equation represents a sufficiently accurate fit of the results for ultimate capacity:

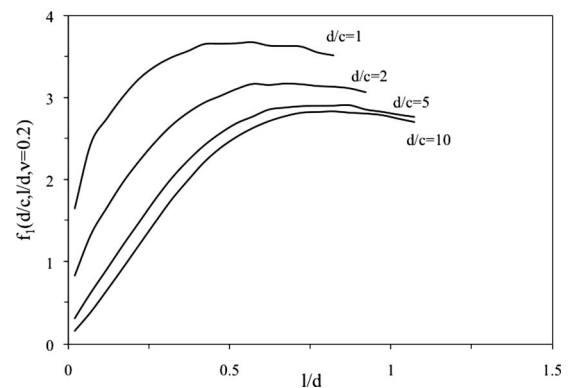


Fig. 6. Function f_1 as functions of crack length and embedment depth

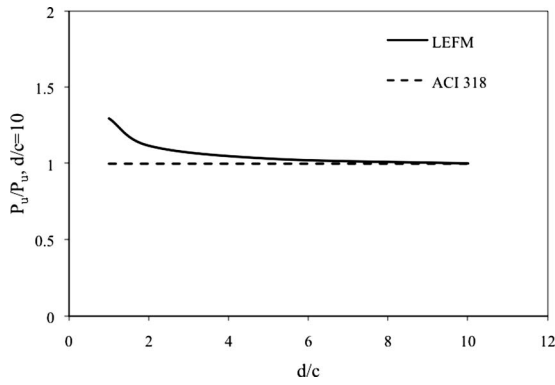


Fig. 7. Ultimate load P_u normalized by the ultimate load for a normal anchor embedded at a normalized depth $d/c=10$, unstressed matrix

$$\frac{P_u}{f_t d^2} = \frac{3.15}{\sqrt{\beta}} + 0.53\lambda \quad (7)$$

Eq. (7) provides a basis for the development of a design formula for ultimate capacity that accounts for prestress. For $\beta=2.5$ a modest but significant increase of the order of 15–20% is achieved for the largest value of prestress of practical relevance, $\lambda \sim 0.4-0.6$. For tensile prestress, the model predicts that for $\beta=2.5$ and $\lambda=-0.6$ there is a reduction in ultimate load capacity of the order of 25–30%.

Ultimate Load-Carrying Capacity: Experimental Program

The experimentally measured normalized ultimate capacity data for unstressed and prestressed concrete are shown in Fig. 8. The ultimate capacity was nondimensionalized using the measured uniaxial tensile strength, f_t [417 psi (2.88 MPa)], of the material, and values of $d=0.98$ in. (24.89 mm) for $d/c=1$ and $d=1.96$ in. (49.78 mm) for $d/c=2$. It is remarkable, as shown in Fig. 8(b), that the linear dependence on prestress predicted by LEFM (which neglects the presence of the process zone and size dependent fracture toughness) is consistent with the experimental results.

Ultimate Load-Carrying Capacity: Discussion

As aforementioned, the brittleness number was first introduced in the concrete community studies of edge-edge crack beams, where the characteristic length L in Eq. (3) is taken as the beam depth.

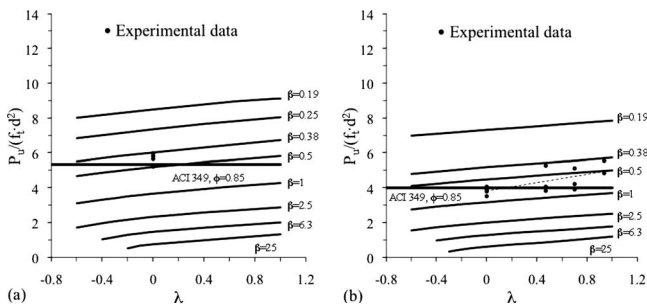


Fig. 8. Ultimate dimensionless pullout load as functions of stress: (a) $d/c=1$; (b) $d/c=2$

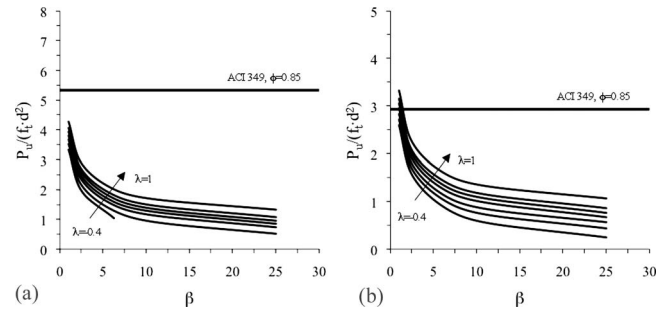


Fig. 9. Ultimate dimensionless pullout load as functions of brittleness: (a) $d/c=1$; (b) $d/c=10$

Typical values of β for edge-edge crack beams therefore range between 2.5 and 10 (Bazant and Planas 1998; Carpinteri 1982). In this study we arbitrarily assign the embedment depth, d , as the characteristic dimension L in Eq. (3). Because of their arbitrary definition, the brittleness numbers discussed subsequently should not be directly related to those of previously reported beam-like specimens.

A comparison between the model's predictions and the experimental results can be achieved by determining a reference value of β . This can be achieved in two ways. The first involves the choice $\beta \approx 0.38$ that bounds from above all the experimental data shown in Fig. 8(b). This value of brittleness is associated with a value of concrete fracture toughness of about $0.95 \text{ ksi}\sqrt{\text{in.}}$, that is well within the range of typical values (between 0.18 and $1.26 \text{ ksi}\sqrt{\text{in.}}$). Having decided to arbitrarily define L as the embedment depth, d , the single experimental data point in Fig. 8(a) ($d/c=1$) is compared with the LEFM prediction associated with $\beta=0.19$. It is observed that the experimental data are, as expected, bounded from above with the LEFM prediction.

The second choice involves choosing a brittleness value $\beta=0.5$ for $d/c=2$ that provides the best least-square fit to the data presented in Fig. 8(b). Then the single data point in Fig. 8(a) is compared with the LEFM prediction for $\beta=0.25$.

With either of the aforementioned choices, it is concluded that the LEFM model represents a close upper bound solution only for relative embedment depths greater than $d/c=2$; for smaller embedment depths the solution becomes unconservative. This corroborates previous experimental investigations and is consistent with Fig. 7, according to which LEFM is not a plausible tool to determine the ultimate load capacity of relatively shallow-headed anchors ($d/c < 2$).

Ductility

The effects of prestress and tensile stresses on ductility are quantified using the work of fracture (WOF), defined as the area under the force-displacement curve. The load-point displacement, Δ , in the simulations is defined as the relative displacement between the top and the bottom surfaces of the discontinuity defining the anchor [Fig. 2(a)]. This displacement cannot be measured in the experiments. Instead the displacement is measured by the two LVDTs positioned symmetrically with respect to the axis of the anchor (Fig. 3). In the subsequent discussion the comparison between the simulated and experimentally measured WOF is therefore qualitative. The normalized WOF for both can be written as

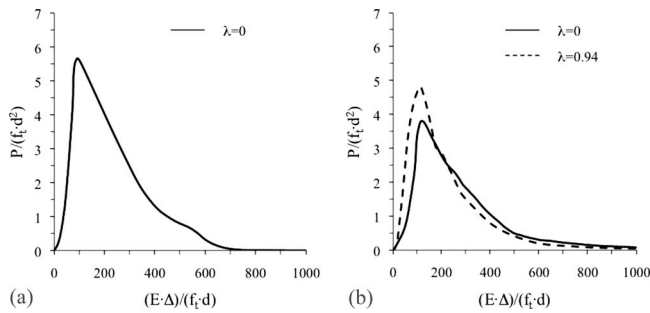


Fig. 10. Load displacement plots from experiments: (a) $d/c=1$; (b) $d/c=2$

$$\text{WOF}_n = \frac{E}{f_t^2 \cdot d^3} \text{WOF} = \int_0^{\Delta_{\max}} \left(\frac{P}{f_t d^2} \right) d \left(\frac{E\Delta}{df_t} \right) \quad (8)$$

and represents the area under the normalized force-displacement curves. When a confining prestress is applied the increase in dissipated energy in the postpeak is large, while the increase in ultimate load is modest. This increase is a result of the significant increase in the length of crack propagation, as shown in the representative plots in Fig. 2(b). The opposite is true for tensile prestressing. As expected, relatively deep embedments and tensile prestress lead to snap-back instabilities in the load-displacement curve.

Even though based on different definitions of the load-point displacement, Δ , Figs. 10 and 11 provide valuable insights. The significant postpeak ductile behavior of the system and the increase in capacity and ductility with the applied compressive stress in the experiments is shown in Fig. 10, where load and displacement were normalized according to the material properties reported in Table 1 and the corresponding embedment depth, d . For a value of $\beta=0.5$, Fig. 11 shows that the LEFM simulations only provide a lower bound solution to the ductility of the

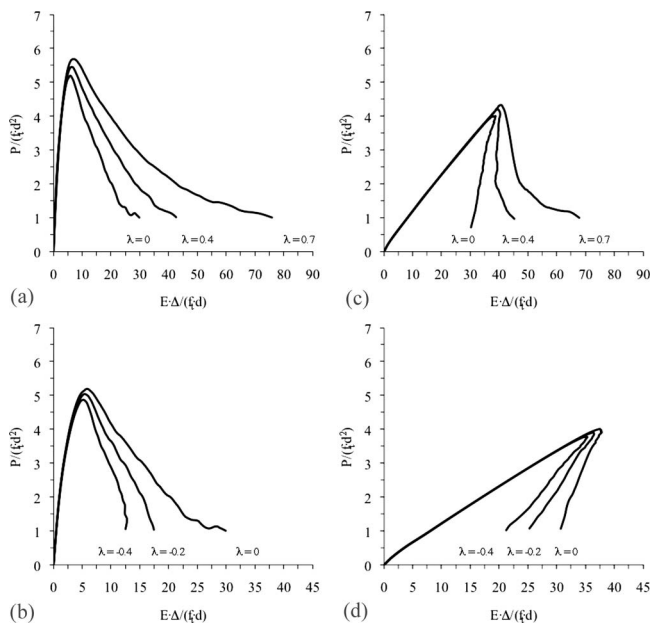


Fig. 11. Load-displacement plots for values of $\lambda=0$, $\lambda=0.4$, $\lambda=0.7$, $\lambda=-0.2$, $\lambda=-0.4$, $\beta=0.5$, and [(a) and (b)] $d/c=1$; [(c) and (d)] $d/c=10$

system and the size of the pullout cone. We note that our crack propagation simulations showed that as the crack approaches the free surface the convergence to zero force is very slow for large values of applied stress. Therefore the curves shown are truncated when the crack front reaches a distance from the free surface that is equal to 10% of the embedment depth.

Conclusions

The incremental discrete crack propagation LEFM results represent a close upper bound solution to the experimentally measured ultimate capacities of anchors embedded in prestressed concrete only at a depth twice the anchor diameter ($d/c=2$). Determination of the capacity of anchors embedded at smaller depths requires nonlinear fracture mechanics modeling. The formulas presented in this paper can be used as a basis for establishing design guidelines for anchors embedded in prestressed concrete.

When tension is applied, the weakening nature of tensile stresses produces a decrease in ultimate load capacity and ductility of headed anchors. For selected values of tension, a 25–30% decrease in load-carrying capacity and a much larger decrease in WOF and in the size of the pullout cone are observed relative to an unstressed matrix. These results only partially agree with the actual code provisions for anchors installed in cracked concrete, where a capacity reduction of about 25–30% is predicted for values of tension close to the tensile strength of the concrete ($\lambda \approx -1$). In addition to the fact that the results from the LEFM analyses are representing only a qualitative solution, this shows that the actual code provisions and test setups, where a precracked reinforced concrete matrix is externally restrained to control the crack width during the anchors extraction, might be suitable to predict the effects of concrete cracking and not the effects of pure applied tensile fields without any restraint.

Acknowledgments

The experimental part of this research was carried out with the support of Yucatan Decima concrete precast plant and its technical staff. The staff of the Laboratorio Prove Materiali of the Politecnico di Milano is also gratefully thanked. The writer expresses his gratitude to the cowriters, to professors L. Biolzi and G. Rosati, and to D. Spinelli for their valuable advice, constant encouragement, and tireless dedication.

References

- ACI Committee 318. (2008). "Building code requirements for structural concrete (ACI 318-08) and commentary (318R-08)." American Concrete Institute, Detroit.
- ACI Committee 349. (1989). "Code requirements for nuclear safety." Appendix B, steel embedments, manual of concrete practice, part IV, ACI #349.1R, American Concrete Institute, Detroit.
- ACI Committee 349. (2006). "Code requirements for nuclear safety related concrete structures (ACI 349-06) and commentary (349R-06)." Appendix D, anchoring to concrete, American Concrete Institute, Detroit.
- ASTM. (1996). "Standard test method for splitting tensile strength of cylindrical concrete specimens." *ASTM C496/C496M*, West Conshohocken, Pa.
- ASTM. (2002). "Standard practice for making and curing concrete test specimens in the field." *ASTM C31/C31M*, West Conshohocken, Pa.

- Ballarini, R., Keer, L. M., and Shah, S. P. (1987). "An analytical model for the pull-out of rigid anchors." *Int. J. Fract.*, 33(2), 75–94.
- Ballarini, R., Shah, S. P., and Keer, L. M. (1985). "Failure characteristics of short anchor bolts embedded in a brittle material." *Proc. R. Soc. London*, A404, 35–54.
- Baran, E., Schultz, A. E., and French, C. E. (2006). "Tension tests on cast-in-place inserts: The influence of reinforcement and prestress." *PCI J.*, 51(5), 88–108.
- Barsoum, R. S. (1976). "On the use of isoparametric finite elements in linear fracture mechanics." *Int. J. Numer. Methods Eng.*, 10(1), 25–37.
- Bazant, Z. P., and Planas, J. (1998). *Fracture and size effect in concrete and other quasibrittle materials*, CRC, Boca Raton, Fla.
- Broek, D. (1986). *Elementary engineering fracture mechanics*, Martinus Nijhoff, Dordrecht, The Netherlands.
- Carpinteri, A. (1982). "Notch sensitivity in fracture testing of aggregate materials." *Eng. Fract. Mech.*, 16(4), 467–481.
- Cattaneo, S. (2007). "Wedge-type expansion anchors in high-performance concrete." *ACI J.*, 104(2), 191–198.
- Cherepanov, G. P. (1979). *Mechanics of brittle fracture*, McGraw-Hill, New York.
- Comité Euro-International du Béton (CEB). (1997). *Design of fastenings in concrete, design guide*, Thomas Telford, London.
- Elfgren, L. (1998). "Round robin analyses and tests of anchor bolts in concrete structures." *RILEM technical committee 90-FMA: Fracture mechanics of concrete applications*, RILEM, Cachan Cedex, France.
- Elfgren, L., and Ohlsson, U. (1992). "Anchor bolts modeled with fracture mechanics." *Application of fracture mechanics to reinforced concrete*, A. Carpinteri, ed., Elsevier Applied Science, London, 267–283.
- Eligehausen, R., and Balogh, T. (1995). "Behavior of fasteners loaded in tension in cracked reinforced concrete." *ACI J.*, 92(3), 365–379.
- Eligehausen, R., Malleé, R., and Silva, J. (2006). *Anchorage in concrete construction*, Ernst and Sohn Publishers, Berlin.
- Eligehausen, R., Mattis, L., Wollmershauser, R., and Hoehler, M. (2004). "Testing anchors in cracked concrete." *Concr. Int.*, 26(7), 66–71.
- Eligehausen, R., and Sawade, G. (1989). "Analysis of anchorage behaviour (literature review)." *Fracture mechanics of concrete structures: From theory to applications*, L. Elfgren, ed., Chapman & Hall, London, 263–280.
- Farrow, C. B., Frigui, I., and Klinger, R. E. (1996). "Tensile capacity of single anchors in concrete: Evaluation of existing formulas on an LRFD basis." *ACI J.*, 91(2), 128–137.
- Farrow, C. B., and Klinger, R. E. (1995). "Tensile capacity of anchors with partial or overlapping failure surfaces: Evaluation of existing formulas on an LRFD basis." *ACI J.*, 92(6), 698–710.
- FRANC-2D. (1997). "Cornell Fracture Group home page." (http://www.cfg.cornell.edu/software/franc2d_casca.htm).
- Fuchs, W., Eligehausen, R., and Breen, J. E. (1995). "Concrete capacity design (CCD) approach for fastening to concrete." *ACI J.*, 92(1), 73–94.
- Karihaloo, B. L. (1996). "Pull-out of axisymmetric headed anchors." *Mater. Struct.*, 29(3), 152–157.
- Klinger, R. E., and Mendonca, J. A. (1982). "Tensile capacity of short anchor bolts and welded studs: A literature review." *ACI J.*, 79(27), 270–279.
- Krenchel, H., and Shah, S. P. (1985). "Fracture analysis of the pullout test." *Mater. Struct.*, 18(6), 439–446.
- Ozbolt, J., and Eligehausen, R. (1992). "Fastening elements in concrete structures—Numerical solutions." *Proc., Fracture of Concrete and Rock, 2nd Int. Conf.*, H. P. Rossmanith, ed., E & FN Spon, London, 527–547.
- Ozbolt, J., Eligehausen, R., and Reinhardt, H. W. (1999). "Size effect on the concrete cone pull-out load." *Int. J. Fract.*, 95(1–4), 391–404.
- Vogel, A., and Ballarini, R. (1999). "Ultimate load capacities of plane and axisymmetric headed anchors." *J. Eng. Mech.*, 125(11), 1276–1279.